Available online at www.CivileJournal.org

Civil Engineering Journal

(E-ISSN: 2476-3055; ISSN: 2676-6957)

Vol. 12, No. 06, June, 2026

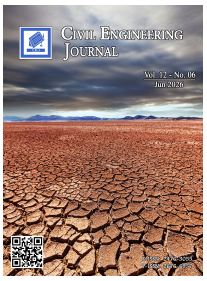

Crossflow Thermoelectric Kitchen Hood System for Enhancing Sustainable Energy in Buildings

Eki Rovianto [1], Rezi Delfianti [2*], Federico Minelli [3], Catur Harsito [1, 4], Rakesh Podder [5], Salaki Reynaldo Joshua [6]

[1] *Department of Mechanical Engineering, Vocational School, Universitas Sebelas Maret, Surakarta 57126, Indonesia.*

[2] *Faculty of Advanced Technology and Multidiscipline, Airlangga University, Surabaya 60115, Indonesia.*

[3] *Department of Industrial Engineering, University of Naples Federico II, 80138 Naples, Italy.*

[4] *Department of Mechanical Computer Industrial Management Engineering, Kangwon National University, Samcheok 25913, South Korea.*

[5] *Department of Computer Science, Colorado State University, Fort Collins, CO, 80523, United States.*

[6] *Department of Informatics Engineering, Sam Ratulangi University, Manado 95115, Indonesia.*

Received 02 August 2025; Revised 24 April 2026; Accepted 03 May 2026; Published 01 June 2026

Abstract

Thermoelectric devices are capable of converting thermal energy into electrical energy. Waste heat recovery can be effectively achieved using thermoelectric modules. This study investigates the performance of thermoelectric generators integrated into a ducting-based kitchen hood system, with a focus on the impact of inlet temperature. A numerical simulation approach was employed and validated through comparison with previous studies. The validation results indicate a low error margin, with an error value below 5%. Simulations were conducted using ANSYS to analyze the effects of hot and cold airflow within a cross-section system. A steady-state simulation approach was employed to evaluate the thermal and fluid dynamic behavior of the system. Tetrahedral meshing was applied, resulting in a total of 25×10^6 elements. The simulation results revealed that the temperature difference distribution formed a descending diagonal pattern from the lower-left to the upper-right region, which significantly influenced the output power generation of the system. The highest observed temperature difference was 313 K, while the lowest was 113 K, with the maximum power output recorded at 0.1903 W. The total power generated by the system, representing the cumulative output from all thermoelectric modules, reached 19.03 W at an inlet temperature of 600 K. The corresponding system efficiency was calculated to be 2.75%. These results indicate that inlet temperature significantly influences the generated power. Further studies investigating the combined effects of airflow velocity and inlet temperature are recommended to optimize system performance and enhance thermal-to-electric energy conversion efficiency. Additionally, experimental investigations are suggested as a means of further validation under real-world operating conditions.

Keywords: Energy Harvesting; Optimization; Thermoelectric Generator; Inlet Air Temperature; Energy in Buildings; Renewable Energy.

1. Introduction

The continuously increasing global energy demand, coupled with growing awareness of the importance of renewable energy utilization, has driven various efforts to optimize the use of alternative energy sources [1–3]. One of the most underutilized forms of energy is waste heat, which is commonly generated from industrial processes, building cooling

* Corresponding author: rezi.delfianti@ftmm.unair.ac.id

https://doi.org/10.28991/CEJ-2026-012-06-014

systems, and household activities such as cooking [4, 5]. Converting waste heat into electrical energy represents a promising pathway to support the transition toward sustainable energy systems [6, 7].

Thermoelectric (TE) technology offers a direct approach to converting heat into electrical energy through the Seebeck effect, without the need for moving components, making it low-maintenance and environmentally friendly [8, 9]. Various studies have been conducted to improve the performance of thermoelectric systems, including material selection, optimization of thermoelectric leg geometry (such as sandwich leg designs), and integration with cooling systems to maintain an optimal temperature gradient [10].

One of the recent approaches involves the application of thermoelectric technology in small-scale waste heat systems, such as photovoltaic-thermoelectric (PV-TEG) hybrids and campfire-powered devices for forest exploration [11]. Savescu et al. [12] extended this concept to industrial auxiliaries, demonstrating with coupled infrared thermography and COMSOL modeling that a twin-screw compressor's casing can sustain $\Delta T \approx 2.5$ °C and deliver ≈1.5 V per 40 mm Bi_2Te_3 module without exceeding vibration-induced stress limits, thereby validating compressors as viable low-grade heat sources for micro-power harvesting systems. These studies indicate that, despite the moderate nature of heat sources, thermoelectric systems can provide a significant energy gain, with efficiency that can be further improved through structural engineering of TE legs and the selection of appropriate materials.

In domestic environments, kitchen hoods generate a substantial and continuous supply of waste heat that is rarely utilized. Recent studies have examined the potential of harnessing this energy using thermoelectric generators (TEGs) based on Bi_2Te_3, showing that leg aspect ratio and temperature distribution strongly affect power output [13]. One experimental setup, for example, converted 6,713 W of heat into only 11.19 W of electricity, yielding a low efficiency of about 0.17%, which underscores the need for further design optimization. Previous simulations often applied uniform boundary temperatures to the hot and cold sides of the module, a simplification that does not capture real airflow effects. Therefore, it was necessary to examine the effect of airflow across the integrated thermoelectric surface, resulting in a more realistic temperature gradient. This CFD-based steady-state approach provides a more accurate prediction of heat distribution and power output, supporting the development of more efficient and sustainable thermoelectric kitchen hood systems.

Moreover, the use of composite materials such as BiSbTe, PbTeS, and SnSe in TEG systems has demonstrated improved efficiency within the medium temperature range, aligning well with the thermal characteristics of kitchen hood systems [14]. Numerical simulation using ANSYS software has become a primary method in these studies for predicting temperature distribution, heat flux density, and potential power output [15, 16]. In this case, it is still limited to numerical simulations on a single module.

Despite numerous studies, the utilization of domestic waste heat; particularly from kitchen hood systems, remains largely underexplored in a comprehensive manner. Existing research tends to focus more on industrial-scale applications, large building energy systems, or even automotive waste heat recovery [17]. In fact, the heat generated from household cooking activities produces a considerable and regular thermal energy flux, making it a potentially stable and sustainable alternative energy source if properly harnessed. Moreover, the direct relationship between temperature difference variation (ΔT) and thermoelectric performance output under constant airflow velocity conditions in kitchen hood systems has not been extensively examined in detail. A thorough understanding of the ΔT factor is essential for designing an optimal thermoelectric system, as ΔT serves as a key parameter that determines the magnitude of voltage, current, and electrical power generated by the thermoelectric module [18].

Therefore, this research aims to evaluate the effect of inlet temperature difference (ΔT) variations on the performance of thermoelectric modules in a kitchen hood system. A CFD-based numerical simulation using ANSYS was conducted to obtain temperature distribution and heat flux characteristics. The electrical power output was evaluated based on variations in ΔT under constant hot and cold airflow velocities. This study is expected to contribute to the development of more efficient thermoelectric-based kitchen hood designs and to support sustainable energy initiatives. The structure of this article is as follows: section 2 explains the methodology, boundary conditions and mesh independent validation in numerical simulations, section 3 presents the results and discussion, and section 4 contains the conclusions and directions for further research.

2. Methodology

2.1. Research Design

This research employs a numerical simulation approach based on Computational Fluid Dynamics (CFD), using ANSYS software to evaluate the effect of inlet temperature variations on the performance of thermoelectric modules in a kitchen hood system. The horizontal duct for hot airflow generated from cooking activity is represented by L_e while the vertical duct for cold airflow from the outdoor environment is represented by L_f and the thermoelectric module is positioned between the two ducts to utilize the temperature difference, with a width of H with the thickness of the hot airflow denoted as d_f and the cold airflow as d_e. The design of the ducting and thermoelectric system is illustrated in Figure 1.

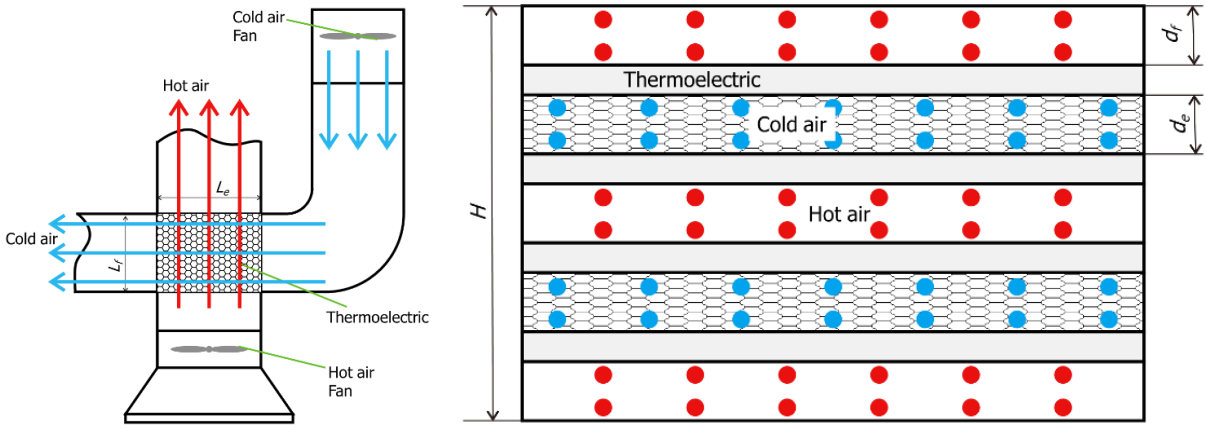

Figure 1. Design of ducting system

The research workflow is illustrated in Figure 2, beginning with the design of the kitchen hood system and its geometry. Once the design and configuration are established, the CFD simulation setup is conducted by defining the fluid material properties and boundary conditions to enable the simulation process. The complete simulation parameters are presented in Table 1. The simulation was then performed using ANSYS software, targeting the objectives outlined in Table 2. Upon completion, a post-processing stage was conducted to analysis the temperature and velocity contours, as well as to estimate the power generated for each variation. The thermoelectric output power was estimated based on the temperature difference and the material properties used, with the calculation method adapted from previous studies [19]. In this case, the generated power was calculated based on the total surface area, which was then divided into smaller segments corresponding to the size of individual thermoelectric modules, and subsequently summed. An analysis was then conducted to evaluate the influence of inlet temperature differences on the resulting power output under a constant inlet velocity.

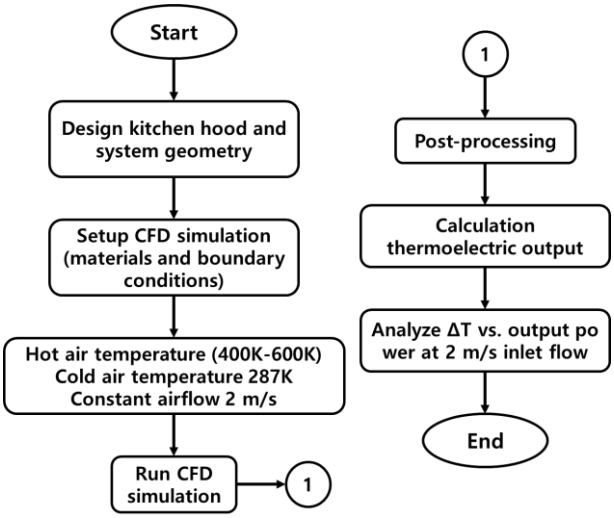

Figure 2. Flow chart of research

Table 1. CFD and Thermoelectric Simulation Parameters

Parameters	Specifications
Fluid	Air (ideal gas), incompressible
Module	Energy + laminar / k-ε turbulence
Material Thermoelectric	Bi_2Te_3
Boundary inlet hot	Temperature: 400K–600K, velocity: 2 m/s
Boundary inlet cold	Temperature: Constant temperature at 287K, velocity: 2 m/s
Outlet	Pressure outlet (0 Pa gauge)
Wall	No slip, adiabatic (except on thermoelectric surfaces)
Mesh	Refined mesh near TE module and boundary layers
Type	Steady-state simulation

Table 2. Experimental Design

No.	Hot Temperature (K)	Cold Temperature (K)	ΔT (K)	Velocity (m/s)
1	400	278	100	2
2	450	278	150	2
3	500	278	200	2
4	550	278	250	2
5	600	278	300	2

2.2. Thermoelectric Power Calculation

The theoretical framework of this research is grounded in the coupling of heat transfer and thermoelectric principles. The temperature difference across the thermoelectric modules is established by the hot and cold air streams flowing on opposite sides of the device. Heat transfer from the hot-side airflow to the module surface, and from the module to the cold-side airflow, is governed by forced convection, which can be expressed as:

$$Q = h.A.\Delta T \tag{1}$$

where, Q is the heat transfer rate, h is the convective heat transfer coefficient, A is the heat transfer area, and ΔT is the local temperature difference between the airflow and the module surface. The convective heat transfer coefficient depends on airflow velocity and fluid properties, while the resulting spatially varying temperature field creates non-uniform thermal gradients across the module surfaces. These gradients directly determine the voltage generated through the Seebeck effect.

In this study, the thermoelectric modules were arranged in a parallel configuration within the system, as illustrated in Figure 1. Each module area experiences a varying temperature difference due to the influence of the airflow. Power output was calculated based on the non-uniform temperature distribution across the module surfaces. Due to these temperature gradients, the electrical voltage generated is governed by the Seebeck effect [20]:

$$V_i = S_i \times \Delta T_i \tag{2}$$

where, V_i is the output voltage of each thermoelectric, S_i the Seebeck coefficient of each thermoelectric, ΔT_i is the temperature difference across the module. Theoretically, in a parallel configuration, the total voltage corresponds to the highest individual voltage; however, in practice, the voltage across parallel modules tends to equalize due to current redistribution. Consequently, the total system current is the sum of the individual module currents. Therefore, the electrical power for each module is calculated individually and then summed to obtain the total system power [21]:

$$P_i = \frac{{V_i}^2}{R_i} = \frac{(S_i \times \Delta T_i)^2}{R_i} \tag{3}$$

where, R_i is the internal electrical resistance of the thermoelectric module. The total electrical power of the system is obtained by summing the power output of all individual modules. This approach accounts for the non-uniform thermal conditions across each module, delivering a more accurate representation of the actual system performance [22]:

$$P_{total} = \sum_{i=1}^{n} \frac{(S_i \times \Delta T_i)^2}{R_i} \tag{4}$$

The efficiency value of this system can be calculated as a whole using the following equation [23]:

$$\eta_{total} = \frac{P_{total}}{Q_{in,\ total}} \times 100\% \tag{5}$$

In this work, the Seebeck coefficient and internal resistance values for Bi_2Te_3 were obtained from literature [4], and they were treated as constant average values within the operating temperature range considered in the simulation.

2.3. Pre-Processing

The initial stage of numerical simulation is to prepare the geometry model, simulation domain, meshing settings and also boundary conditions, where the shape of the three-dimensional geometry model is an aspect that must be considered.

In this study, three-dimensional design is carried out on the space claim menu. This model consists of two fluid flows, namely hot fluid (red) and cold fluid (blue). In addition, in the middle between the hot fluid and the cold fluid there is a thermoelectric module. The fluid domain is used in this simulation on hot and cold air ducts. Meshing is done by ANSYS meshing with tetrahedral elements and the total elements are 25,216,000 as shown in Figure 3. The boundary conditions in this study include inlet temperature (hot and cold), air flow velocity (hot and cold), zero pressure outlet and ducting walls which are assumed to be adiabatic nonslip as shown in Figure 4. Due to device limitations and to minimize simulation time, the simulation conditions are set at a steady state but capture key physical phenomena relevant to system performance. Furthermore, the steady-state approach was chosen because the airflow operates continuously and relatively stable.

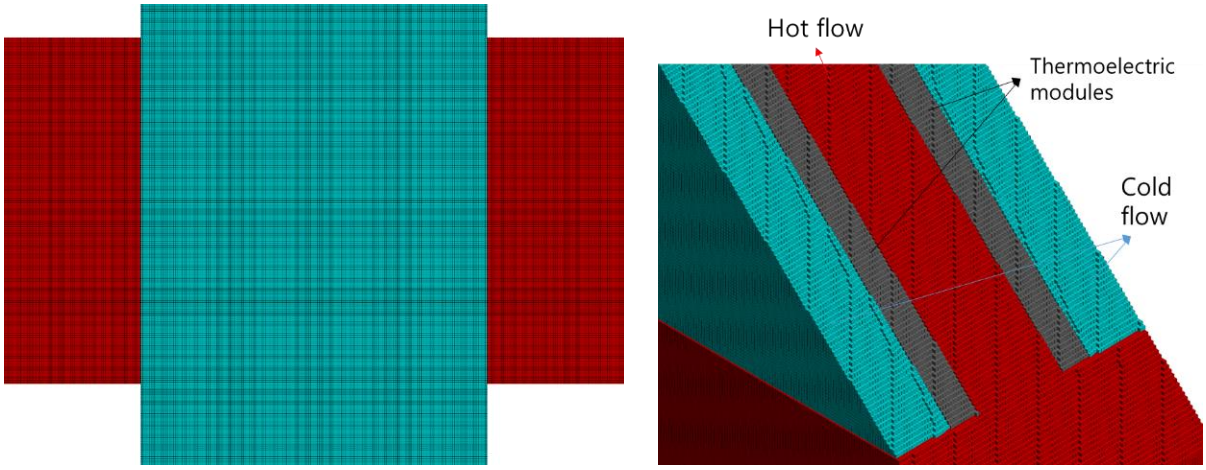

Figure 3. Meshing

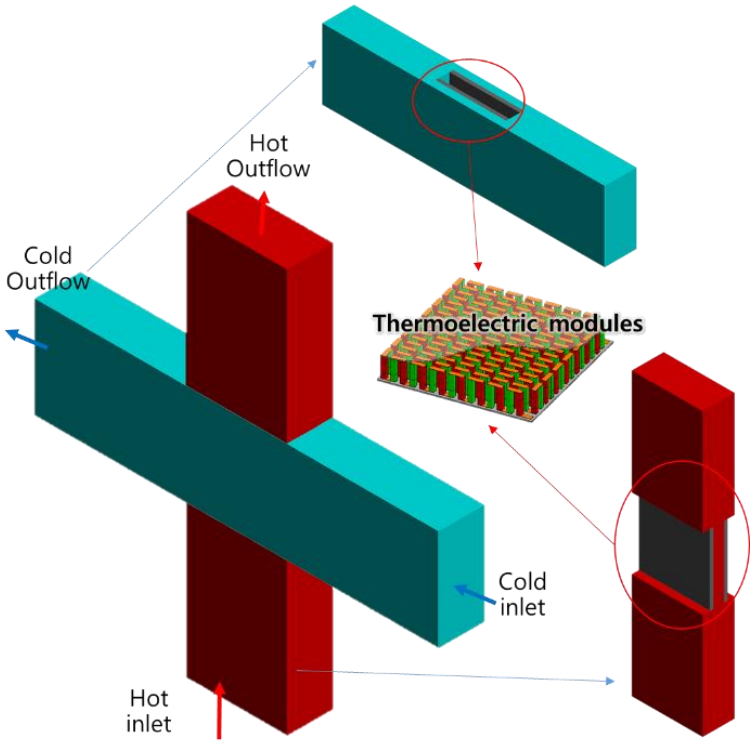

Figure 4. Boundary condition

2.4. Simulation Validation

Mesh independent test is conducted to verify that the model used is not affected by the number of meshes and mesh size. As shown in Figure 5, when the number of meshing is more than $15e^6$ the power output value does not change significantly and is relatively stable. So, it can be concluded that the use of the minimum number of meshing is $15e^6$, and in this study the number of meshing is determined at $25e^6$. This is in accordance with previous research that a model

can be said to be stable when the amount of meshing no longer has a significant influence on the simulation results or it can be said that the error value is low [24]. Since the accuracy of the simulation outcomes is influenced by the amount of iterations, the simulation process also determines the RMS residual level of $10e^{-4}$ [25].

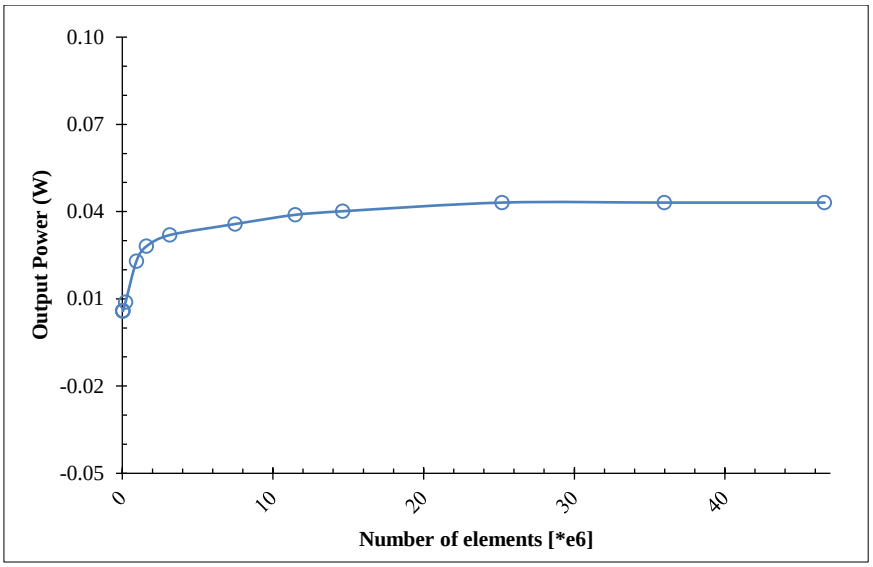

Figure 5. Independent test

Validation is done to test whether the parameters, models and boundary conditions used are running well and are reliable. This validation is done by comparing the simulation results and previous research results with a similar parameter approach so that the research results can be accepted scientifically. The simulation results conducted by Pramudi et al. (2024) which investigated the performance of thermoelectric modules with several different material conditions were used as a comparison [26]. Based on Figure 6 and Table 3, the simulation results show that the output power values obtained are very close to the values produced by previous studies. The differences are below 5% so that they are within reasonable tolerance limits for CFD-based simulations [27]. So, it can be concluded that the simulation provides accurate and scientifically valid results and can be used to carry out further analysis.

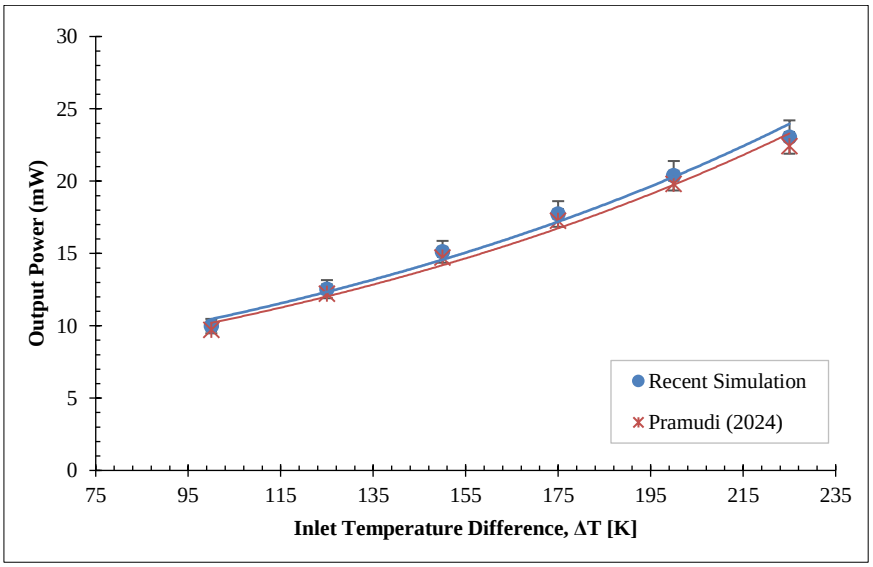

Figure 6. Validation

Table 3. Validation

	Max. Power
Pramudi et al. (2024) [26]	23.05
Present Simulation	22.41
Error	2.84%

3. Result and Discussion

The developed kitchen hood system model consists of a horizontal duct for hot air flow and a vertical duct for cold air flow, with a thermoelectric module placed between the two. The simulation was carried out with a constant hot and cold air flow velocity of 2 m/s. The hot air temperature was varied at 400K, 450K, 500K, 550K, and 600K, while the cold air temperature was kept constant at 287K.

3.1. Temperature Distribution

The simulation results of the temperature distribution on the hot side and cold side are illustrated in contours. Figure 7 shows the contour distribution on the hot side with variations in inlet temperature with an inlet velocity of 2 m/s. The color gradation shows the temperature range where the blue color indicates a temperature of 300K and the red color 480K. As the inlet temperature increases, the thermoelectric module area becomes higher as indicated by the increasingly red color. This contour pattern is caused by crossflow and the development of a boundary layer along the surface, resulting in a non-uniform temperature distribution. This difference is crucial because it directly impacts temperature differences related to thermoelectric performance. From a design perspective, this finding underscores the importance of temperature control and more even distribution of module airflow, thus maximizing system efficiency.

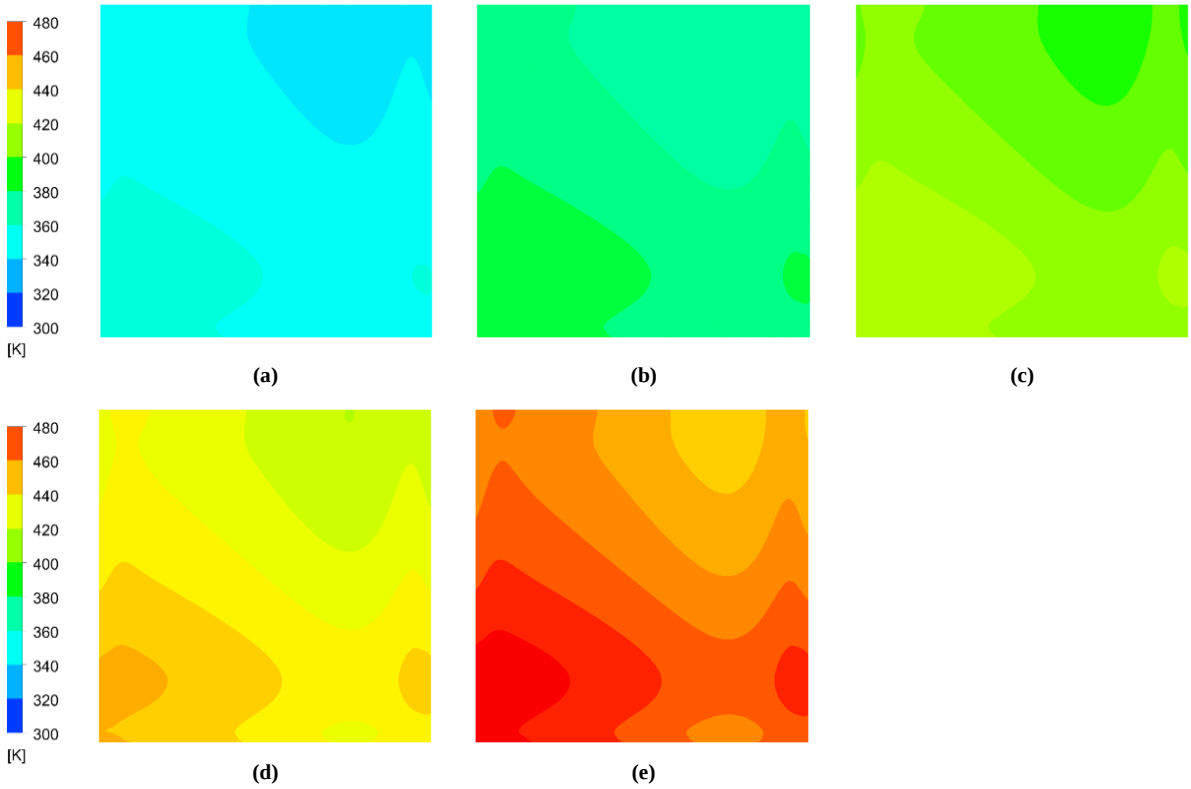

Figure 7. Contour temperature generation on the hot side under varying inlet temperatures at a constant inlet velocity of 2 m/s (a) 400 K; (b) 450 K; (c) 500 K; (d) 550 K and (e) 600 K

Figure 8 shows the temperature contours on the cold side of the system under different inlet temperature conditions. At low inlet temperatures, the contour is dominated by blue, indicating that the cold-side region has a temperature range of 320–360 K. As the inlet temperature increases, the temperature contour shifts from blue to yellow-green and finally to orange, indicating an increase in temperature. The temperature distribution differs clearly under each inlet temperature condition. In Figure 8(e), the highest temperature distribution occurs at the bottom left, while the lowest temperature appears at the top right. This pattern is influenced by the flow directions of the hot and cold air. The hot air flows from bottom to top, whereas the cold air flows from right to left. Similar to the temperature distribution contour on the hot side, the resulting distribution forms a comparable pattern. Cross-flow convection creates variations in temperature differences, which generate electrical voltage through the Seebeck effect. In practical terms, a more uniform flow and temperature distribution are necessary to maximize system efficiency.

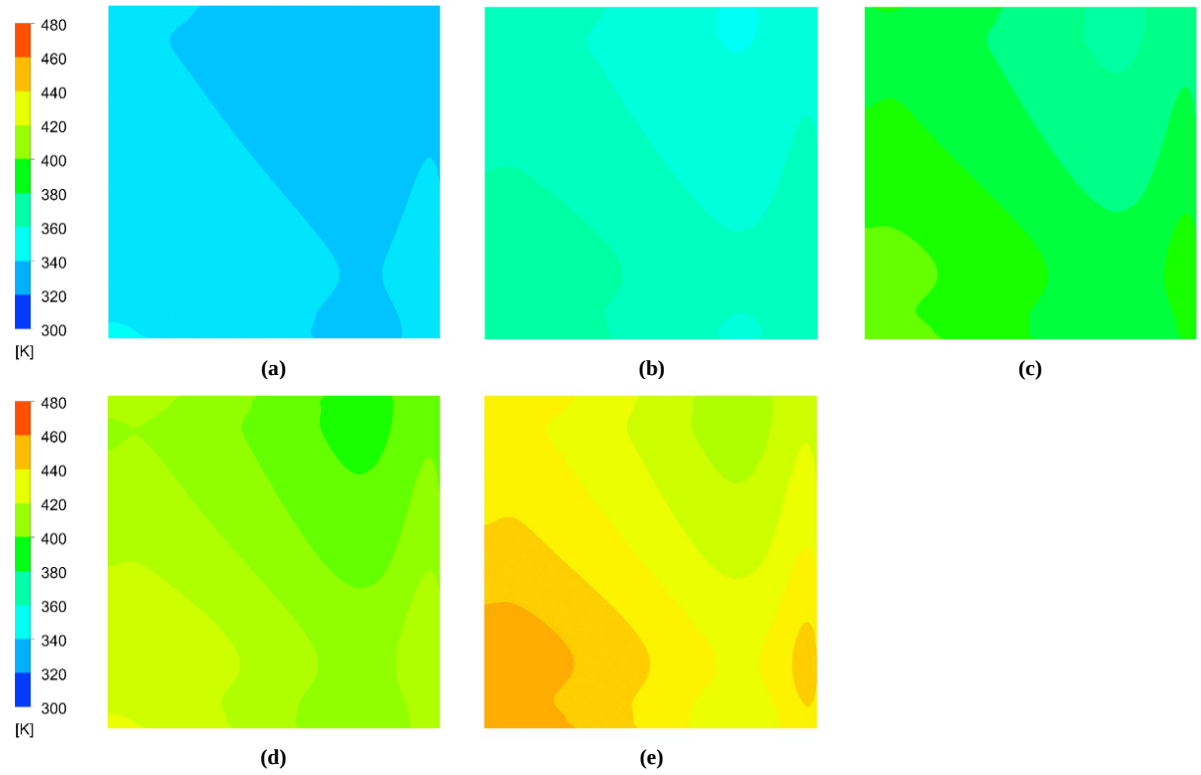

Figure 8. Contour temperature generation on the cold side under varying inlet temperatures at a constant inlet velocity of 2 m/s (a) 400 K; (b) 450 K; (c) 500 K; (d) 550 K and (e) 600 K

3.2. Thermoelectric Output

The thermoelectric output power is predicted based on variations in inlet temperature. The output power is the result of multiplying the thermoelectric efficiency by the heat input, as shown in the five images presented in Figure 9. These contour plots are the results of simulations conducted over a surface area of 400×400 mm. In the images, the blue color represents areas with low heat input, while the red color indicates regions with high heat input. The prediction displayed corresponds to the temperature distribution in each area, which is influenced by the temperature difference between the hot and cold sides.

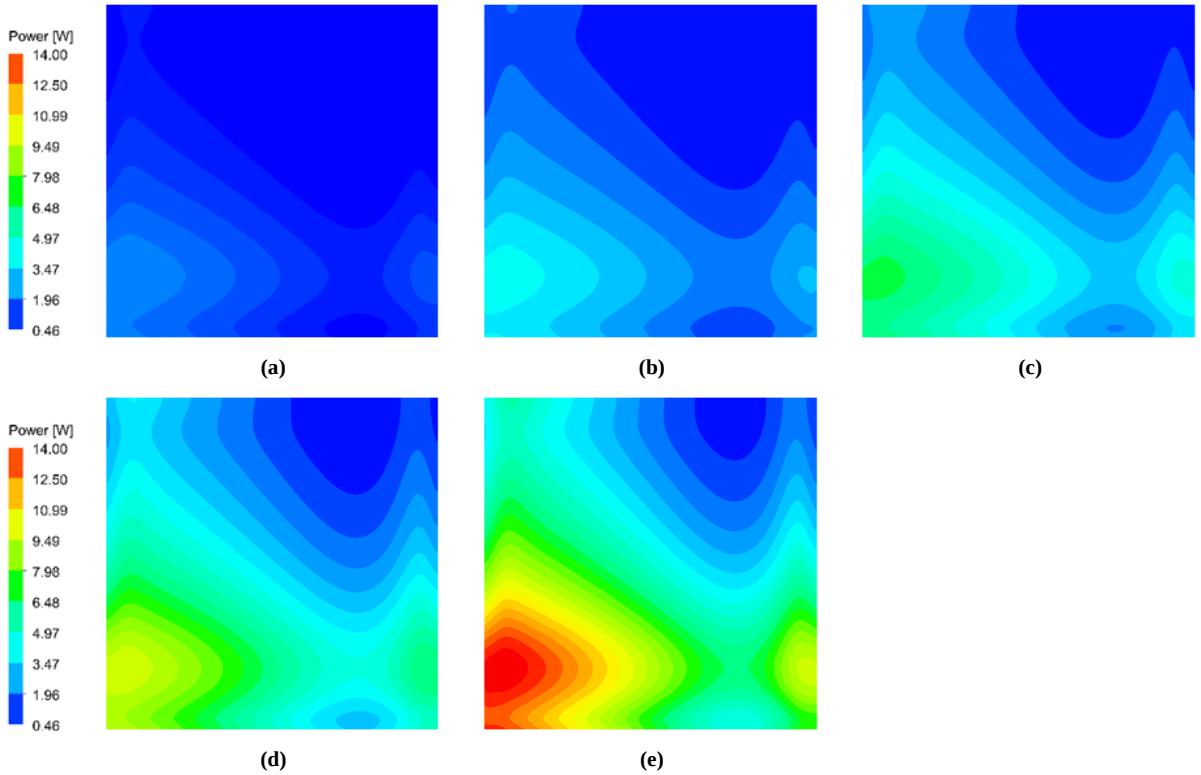

Figure 9. Power generation distribution at an inlet velocity of 2 m/s under varying inlet temperature conditions (a) 400 K; (b) 450 K; (c) 500 K; (d) 550 K and (e) 600 K

In Figure 9-a, the dominance of blue indicates that the heat input is relatively low, which occurs due to the low inlet temperature, resulting in a small temperature difference. In the subsequent images, green and eventually red areas appear, particularly in Figure 9-e, signifying a significant increase in heat input. The power generated is not uniformly distributed across the surface. This is caused by the non-uniform temperature distribution, which itself is caused by cross-flow heat transfer between the hot and cold air streams, leading to spatially varying heat input. The diagonal gradient pattern shown in the images reflects the characteristic behavior of cross-flow configurations, where heat transfer gradually occurs along the interaction path of the flows. Therefore, the resulting power distribution scientifically reflects the interaction between local temperature gradients and the flow direction. It should be noted that this diagonal gradient is a direct consequence of the cross-flow configuration, and geometry modifications (such as the addition of fins, as demonstrated by Yang et al. [28]), could potentially flatten the distribution by promoting a more uniform temperature field across the thermoelectric surface.

Overall, the system's final output power is calculated by summing the power output of each thermoelectric module based on the partial area temperature difference, using Equation 3. The power output for each inlet temperature variation is shown in Figure 10, where increasing the inlet temperature leads to higher output power. This is due to the increased temperature difference.

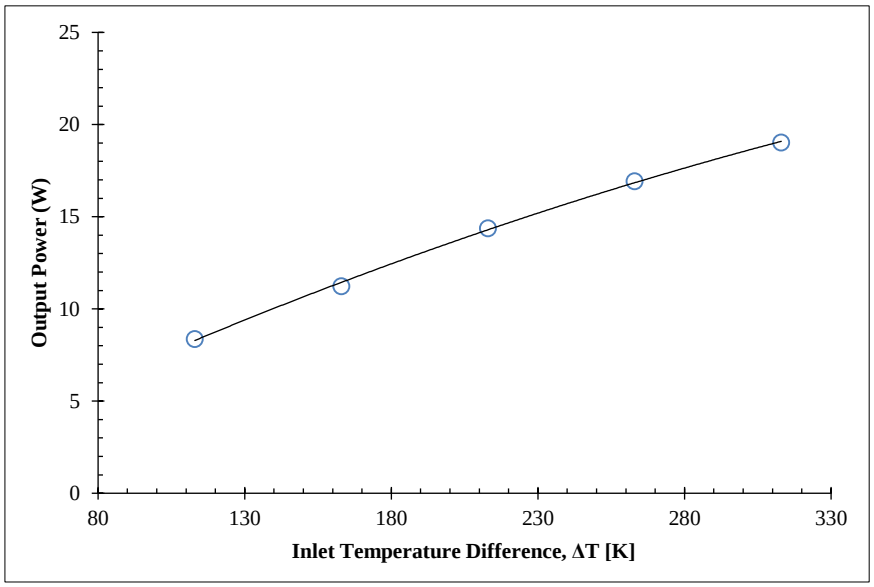

Figure 10. Power generation in thermoelectric-based kitchen hood systems

3.3. Thermoelectric Efficiency

Thermoelectric efficiency is predominantly influenced by the temperature difference (ΔT) between the hot and cold sides of the module. In the present system, this temperature distribution is significantly affected by the cross-flow interaction between hot and cold air streams. The cross-flow configuration creates a dynamic thermal environment where the local heat transfer rate is enhanced due to momentum superposition and pressure gradients at the intersection of the airflow channels. This interaction leads to variations in ΔT across the surface of the thermoelectric modules, ultimately impacting the electrical power output. Numerical simulations revealed that the airflow entering from orthogonal directions generates regions of increased velocity and convective heat transfer, particularly at the central zone where the hot and cold ducts intersect.

Figure 11 illustrates the numerical simulation results of airflow velocity distribution in a three-dimensional domain, clearly depicting regions of accelerated flow at the intersection point of the orthogonal ducts. The velocity contours, ranging from 0 m/s (blue) to 4.3 m/s (red), highlight how the cross-flow effect enhances local convective heat transfer around the thermoelectric module. This phenomenon results in an accelerated flow near the thermoelectric module, improving the local heat exchange and helping to maintain a higher effective temperature difference across the device. As a consequence, the convective enhancement in this area contributes to an increase in the overall thermal efficiency of the system. According to the convection equation, the narrowing of the channel which causes an increase in velocity also affects the resulting temperature distribution, besides increasing the heat transfer that occurs so that the temperature difference between the hot and cold streams is maintained and improves thermoelectric performance.

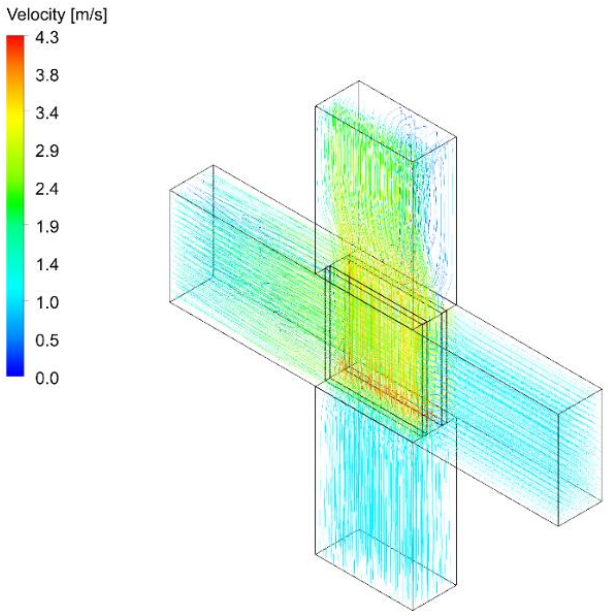

Figure 11. Velocity streamline

The simulations carried out in this study are limited to steady conditions, radiation losses between the fluid flows and the thermoelectric have not been modeled while the resistance in the thermoelectric system is taken into account. The simulation results indicate that as the inlet temperature of the hot air increases, the power output and corresponding system efficiency also increase. Under the highest tested condition (with a hot-side inlet temperature of 600 K and a cold-side temperature maintained at 287 K), the system generated a total power output of 19.03 W, with the maximum output from a single module recorded at 0.1903 W. The corresponding overall system efficiency at this condition was calculated to be 2.75%. The detailed relationship between inlet temperature, power output, and corresponding system efficiency is depicted in Figure 12.

This efficiency value demonstrates a considerable improvement over other low-grade waste heat applications. For comparison, previous studies such as that by Erdogan et al. reported a system efficiency of approximately 1.5% when utilizing 24 commercial Bi_2Te_3 modules on a 290 °C automotive exhaust system. Although their per-module output was slightly higher, the present study demonstrates that kitchen hood waste heat can be harnessed effectively, with competitive system-level efficiency, provided that airflow and thermal conditions are optimized. These findings confirm that cross-flow channel arrangements and high inlet temperatures can substantially enhance thermoelectric performance. They also emphasize the need for continued optimization in geometry, module arrangement, and flow control to maximize waste heat recovery in domestic environments. Further investigation into airflow velocity effects and experimental validation is recommended for practical system deployment.

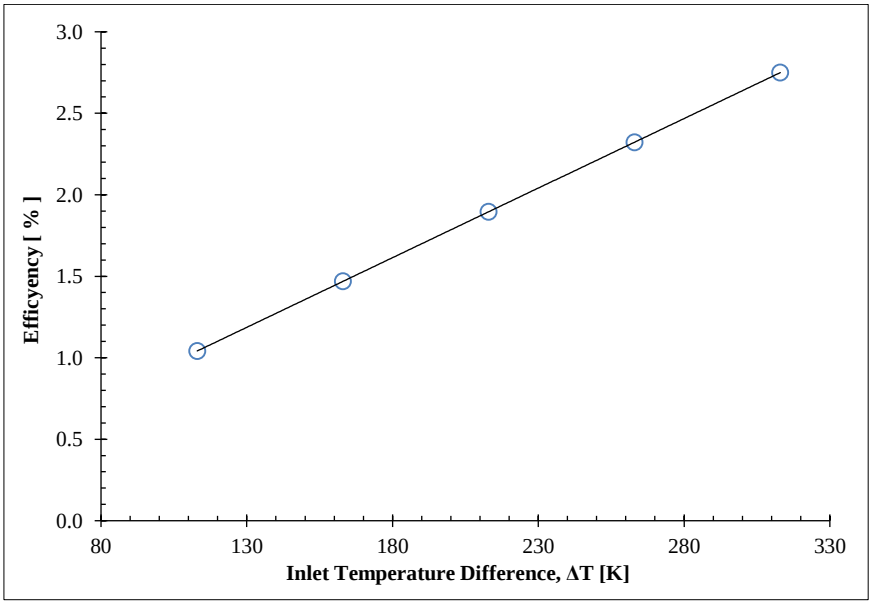

Figure 12. Efficiency of the ducting-thermoelectric system

4. Conclusion

This paper investigates and analyzes the effect of inlet temperature on the performance of thermoelectric generators in kitchen hood ducting systems using a numerical simulation approach. The model was validated and compared with previous studies. The results show that the model has a low error rate; therefore, it can be used to simulate the hot airflow generated by kitchen activities and the cold airflow supplied from outside the room, forming a heat transfer system with a thermoelectric module positioned between them.

Next, the temperature distribution in the area in contact with the thermoelectric module was identified. The results show that the temperature distribution in the contact area with the thermoelectric module is distributed diagonally downward from the bottom left to the top right. This distribution causes differences in the output power generated by each module, with the power output corresponding to the temperature distribution in each area. This diagonal distribution occurs because the hot and cold airflows are combined in a cross-flow system.

The maximum power generated by the module is approximately 0.1903 W, while the total power generated by the system is 19.03 W. The maximum power is obtained when the inlet temperature is set to 600 K. In addition, the overall system efficiency reaches 2.75% at the same inlet temperature. This system can be applied to various systems, but it is more suitable for new installations because it can reduce renovation costs. Overall, the inlet temperature affects the generated power.

It was also found that the velocity increases in the cross-sectional area due to the narrowing of the ducting area. Further studies can be conducted by adding fins or modifying the geometry of the cross-channel to smooth the flow. Additional investigations into the effects of inlet velocity and temperature on both hot and cold airflow are needed to better understand the occurring phenomena and optimize the system to improve heat energy conversion efficiency. Experimental studies can also be conducted for further investigation of this system.

5. Declarations

5.1. Author Contributions

Conceptualization, C.H. and R.D.; methodology, C.H. and E.R.; software, C.H.; validation, C.H., E.R., and F.M.; formal analysis, E.R.; data curation, C.H.; writing—original draft preparation, C.H.; writing—review and editing, F.M., R.D., and C.H.; visualization, R.P. and S.R.J.; supervision, F.M. and R.D. All authors have read and agreed to the published version of the manuscript.

5.2. Data Availability Statement

The data presented in this study are available in the article.

5.3. Funding

The authors received no financial support for the research, authorship, and/or publication of this article.

5.4. Acknowledgments

The authors would like to thank Universitas Sebelas Maret, Airlangga University, Kangwon National University, University of Naples Federico II, Colorado State University and Universitas Sam Ratulangi for laboratory facilities and collaboration research.

5.5. Conflicts of Interest

The authors declare no conflict of interest.

6. References

[1] Delfianti, R., Rovianto, E., Harsito, C., Pradana, J. A., Pongajow, V., & Joshua, S. R. (2024). Daily Electrical Energy Forecasting in Rooftop Photovoltaic Systems: A Case Study. Journal of Soft Computing and Data Mining, 5(2), 197–207. doi:10.30880/jscdm.2024.05.02.015.

[2] Harsito, C., Yun, J. E., Shin, J. Y., & Kim, J. M. (2024). Optimal Design of a Liquid Hydrogen Centrifugal Pump Impeller. Energies, 17(24), 10 3390 17246299. doi:10.3390/en17246299.

[3] Idogho, C., Abah, E. O., Onuhc, J. O., Harsito, C., Omenkaf, K., Samuel, A., Ejila, A., Idoko, I. P., & Ali, U. E. (2025). Machine Learning-Based Solar Photovoltaic Power Forecasting for Nigerian Regions. Energy Science and Engineering, 13(4), 1922–1934. doi:10.1002/ese3.70013.

[4] Yauri, R., Cuyubamba, L., & Nuñez, S. (2025). Crop Monitoring System Using IoT, Solar Energy and Decision Tree Algorithm. Emerging Science Journal, 9(2), 603–614. doi:10.28991/ESJ-2025-09-02-06.

[5] Harsito, C., Muslim, R., Rovianto, E., Kurniawan, Y., & Mahdhudhu, F. M. (2024). Forecasting thermoelectric power generation through utilization of waste heat from building cooling systems based on simulation. E-Prime - Advances in Electrical Engineering, Electronics and Energy, 10, 100821. doi:10.1016/j.prime.2024.100821.

[6] Luo, D., Zhao, Y., Yan, Y., Chen, H., Chen, W. H., Wang, R., Li, Y., & Yang, X. (2023). Development of two transient models for predicting dynamic response characteristics of an automobile thermoelectric generator system. Applied Thermal Engineering, 221, 119793. doi:10.1016/j.applthermaleng.2022.119793.

[7] Lin, Q., Chen, Y. C., Chen, F., DeGanyar, T., & Yin, H. (2022). Design and experiments of a thermoelectric-powered wireless sensor network platform for smart building envelope. Applied Energy, 305, 117791. doi:10.1016/j.apenergy.2021.117791.

[8] Luo, D., Yu, Y., Yan, Y., Chen, W. H., & Cao, B. (2024). Increasing power densities in a thermoelectric generator by stacking and incorporating dual heat pipes. Device, 2(8), 100435. doi:10.1016/j.device.2024.100435.

[9] Gao, Y., Wu, D., Dai, Z., Wang, C., Chen, B., & Zhang, X. (2021). Performance analysis of a hybrid photovoltaic-thermoelectric generator system using heat pipe as heat sink for synergistic production of electricity. Energy Conversion and Management, 249, 114830. doi:10.1016/j.enconman.2021.114830.

[10] Harsito, C., Muslim, R., Rovianto, E., Prasetyo, A. (2024). Investigation of a Thermoelectric Generator with Sandwich Leg Modification. Proceedings of the 9th International Conference and Exhibition on Sustainable Energy and Advanced Materials, ICE-SEAM 2023, Lecture Notes in Mechanical Engineering. Springer, Singapore. doi:10.1007/978-981-97-0106-3_53.

[11] Harsito, C., Purba, D. A., Mufti Reza Aulia, P., Triyono, T., & Permata, A. N. S. (2022). Mini Review of Thermoelectric Application with LFP 18650 Battery in Forest Exploration Campfire. AIP Conference Proceedings, 2499, 0104938. doi:10.1063/5.0104938.

[12] Savescu, C., Petrescu, V., Comeaga, D., Carlanescu, R., Roman, M., Lale, D., & Mitru, A. (2024). Thermal Potential of a Twin-Screw Compressor as Thermoelectric Energy Harvesting Source. Engineering, Technology and Applied Science Research, 14(2), 13449–13455. doi:10.48084/etasr.6417.

[13] Harsito, C., Delfianti, R., Syahroni, R. C., Nusyura, F., & Minelli, F. (2025). Effect of aspect ratio on thermoelectric system performance for waste heat recovery as alternative energy in building. Results in Engineering, 26, 105115. doi:10.1016/j.rineng.2025.105115.

[14] Delfianti, R., Harsito, C., Syahroni, R. C., Nusyura, F., & Minelli, F. (2025). Effect of Geometric Aspect Ratio on the Performance of Thermoelectric Generators for Waste Heat Utilization in Buildings. Journal of Advanced Research in Numerical Heat Transfer, 34(1), 32–42. doi:10.37934/arnht.34.1.3242.

[15] Zhang, N., Wang, J., Li, Y., Lan, J., & Lan, S. (2024). The impact of the heat leakage through air gap on thermoelectric generator applied in engine waste heat recovery. Green Energy and Resources, 2(3), 100088. doi:10.1016/j.gerr.2024.100088.

[16] Permata, A. N. S., Idogho, C., Harsito, C., Thomas, I., & John, A. E. (2025). Compatibility in thermoelectric material synthesis and thermal transport. Unconventional Resources, 7, 100198. doi:10.1016/j.uncres.2025.100198.

[17] Quan, R., Wang, J., Liang, W., Li, X., & Chang, Y. (2024). Numerical investigation of a thermoelectric generator system with embedded sickle-shaped fins. Applied Thermal Engineering, 236, 121741. doi:10.1016/j.applthermaleng.2023.121741.

[18] Kang, Y. K., Joung, J., Kim, M., & Jeong, J. W. (2023). Energy impact of heat pipe-assisted microencapsulated phase change material heat sink for photovoltaic and thermoelectric generator hybrid panel. Renewable Energy, 207, 298–308. doi:10.1016/j.renene.2023.03.042.

[19] Jia, Y., Wang, B., Tian, J., Song, Q., Chen, Y., Zhang, W., Wang, C., Sun, H., & Zhang, Z. (2024). A thermal conductivity varying 3D numerical model for parametric study of a silicon-based nano thermoelectric generator. Energy, 293, 130574. doi:10.1016/j.energy.2024.130574.

[20] Kang, Y. K., Joung, J., Kim, S., Park, J., & Jeong, J. W. (2024). Design of a thermoelectric generator-assisted photovoltaic panel hybrid harvester using microencapsulate phase change material. Journal of Building Engineering, 87, 109110. doi:10.1016/j.jobe.2024.109110.

[21] Alian Fini, M., Gharapetian, D., & Asgari, M. (2022). Efficiency improvement of hybrid PV-TEG system based on an energy, exergy, energy-economic and environmental analysis; experimental, mathematical and numerical approaches. Energy Conversion and Management, 265, 115767. doi:10.1016/j.enconman.2022.115767.

[22] Win, S. L. Y., Chiang, Y. C., Huang, T. L., & Lai, C. M. (2024). Thermoelectric Generator Applications in Buildings: A Review. Sustainability (Switzerland), 16(17), 10 3390 16177585. doi:10.3390/su16177585.

[23] Ji, Y., & Lv, S. (2023). Experimental and numerical investigation on a radiative cooling driving thermoelectric generator system. Energy, 268, 126734. doi:10.1016/j.energy.2023.126734.

[24] Muslim, R., Pramudi, G., Adika, D., & Harsito, C. (2025). Thermoelectric Characteristics of Bi2S3-Based Sandwich Materials. International Journal of Energy Production and Management, 10(1), 107–117. doi:10.18280/ijepm.100111.

[25] Harsito, C., Pramudi, G., Muslim, R., Adika, D., & Kurniawan, Y. (2024). Investigation of Sandwich-Type Generator Thermoelectric Element Power Generation. Engineered Science, 27, 1–8. doi:10.30919/es1016.

[26] Pramudi, G., Harsito, C., Muslim, R., & Adika, D. (2024). Investigation of a Thermoelectric Generator with Sandwich Leg Modification. International Journal on Engineering Applications, 12(2), 87–93. doi:10.15866/irea.v12i2.23648.

[27] Erturun, U., Erermis, K., & Mossi, K. (2015). Influence of leg sizing and spacing on power generation and thermal stresses of thermoelectric devices. Applied Energy, 159, 19–27. doi:10.1016/j.apenergy.2015.08.112.

[28] Yang, S., Chen, H., & Luo, D. (2025). Advanced bifurcated fin design with diversion channels for optimizing output performance of thermoelectric generators. International Communications in Heat and Mass Transfer, 165, 109078. doi:10.1016/j.icheatmasstransfer.2025.109078.